EUROPEAN JOURNAL OF PURE AND APPLIED MATHEMATICS
2026, Vol. 19, Issue 2, Article Number 6239
ISSN 1307-5543 – ejpam.com
Published by New York Business Global

Thermal and Flow Analysis of Nanofluid Flow over a Lubricated Stretched Sheet with Velocity Slip Effects

Ilyas Khan[1,2,3,4,5,6,7,8], Rabia Kamal[9],
Tasawar Abbas[10,*], Zeeshan Ali[11], Mirza Muhammad Tahir[10],
Bilal Ahmad[10], Zaher Mundher Yaseen[12], Wei Sin Koh[13]

[1] *Department of Mathematical Sciences, Saveetha School of Engineering, SIMATS, Chennai, Tamil Nadu, India*
[2] *Department of Mathematics, College of Science Al-Zulfi, Majmaah University, Al-Majmaah 11952, Saudi Arabia*
[3] *Széchenyi István University, Győr, Hungary*
[4] *Irfan Gunsel Operational Research Institute in Healthcare, Near East University, Mersin 10, Nicosia, TRNC, Turkey*
[5] *Faculty of Art and Science, University of Kyrenia, Mersin 10, Nicosia, TRNC, Turkey*
[6] *International Center for Interdisciplinary Research in Sciences, The University of Lahore, Lahore, Pakistan*
[7] *Mathematics in Applied Sciences and Engineering Research Group, Scientific Research Center, Al-Ayen University, Nasiriyah 64001, Iraq*
[8] *Jadara University Research Center, Jadara University, Jordan*
[9] *FG Post Graduate College for Women Wah Cantt, 47040 Pakistan*
[10] *Department of Mathematics, University of Wah, Wah Cantt, 47040 Pakistan*
[11] *Department of Information Management, National Yunlin University of Science and Technology, 123 University Road, Section 3, Douliou, Yunlin 64002, Taiwan, R.O.C*
[12] *Civil and Environmental Engineering Department, King Fahd University of Petroleum and Minerals, Dhahran 31261, Saudi Arabia*
[13] *INTI International University, Persiaran Perdana BBN Putra Nilai, 71800 Nilai, Negeri Sembilan, Malaysia*

*Corresponding Author.
DOI: https://doi.org/10.29020/nybg.ejpam.v19i2.6239

Abstract. This study presents a mathematical model for the two-dimensional flow of a nanofluid over a lubricated stretching sheet with a thin layer of power-law lubrication coating. lubricant layer of varying thickness coat the sheet, impacting the flow dynamics and heat transfer characteristics. Temperature-dependent thermal conductivity, Brownian diffusion, and thermophoresis effects are incorporated into modified governing equations corresponding to mass, momentum, energy, and concentration conservation laws. Key parameters affecting the thermal and solutal gradients in the nanofluid include the ambient and surface temperature, as well as concentration levels. The model accounts for both slip and no-slip boundary conditions due to the lubrication layer, and ensures interfacial shear stress continuity between the nanofluid and lubricant. Recently, heat transfer has been a noticeable enhanced due to nanoparticles interactions. The effect of lubrication phenomena and its impact on heat and mass transmission is crucial. The thermal effect of nanofluid on lubricated stretched surfaces close to a stagnation point has been investigated numerically in recent work. A reliable and effective method, the Keller Box Numerical Scheme, is used to solve the transformed ordinary differential equations (ODEs) in the boundary layer. Based on theoretical flow assumptions, a range of flow parameters is considered. When lubrication is applied, a physical analysis of relevant parameters, including temperature, concentrations, and velocity, is conducted. Slip conditions at the interface between the nanofluid and the power-law lubricant are enforced, incorporating surface slip and the stretching velocity of the sheet. Key parameters, such as the Brownian motion, Prandtl, Eckert, and slip parameter are introduced to study the impact of fluid and thermal characteristics on the system.

2020 Mathematics Subject Classifications: 76D10, 76M20, 80A20, 35Q35

Key Words and Phrases: Power-law lubricant, Lubricated stretching sheet, Nanofluid flow, Energy transition, Temperature-dependent conductivity, Brownian motion, Slip conditions, Velocity slip effects, Keller Box Scheme

1. Nomenclature with Units

Symbols	Description	Units
v	Vertical velocity	m/s
u	Horizontal velocity	m/s
T	Temperature	K
ρ	Base fluid density	Kg/m^3
p	Pressure	Pa
ϕ	Nanoparticle concentration	-
ν	Kinematic viscosity	m^2/s
D_T	hermophoresis coefficient	m^2/s
D_B	Brownian diffusion coefficient	m^2/s
k	Thermal conductivity	$W/(m.k)$
q	Heat flux	W/m^2
Nu	Nusselt number	-
S_h	Sherwood number	-
C_f	Skin friction coefficient	-
Ec	Eckert number	-
Pr	Prandtl number	-
Le	Lewis number	-
Re	Reynolds number	-

2. Introduction

In fluid dynamics, the analysis of the flow encompasses the discussion of the motion of the fluids, the forces involved, and the phenomena they form. Nanofluid can be described as a fluid containing nanoparticles, normally measured between 1-100nm, mixed with the fluid in suspension form. Nanoparticles are mixed in a liquid medium of water, oil, or ethylene glycol to rise the certain properties of the fluid.

Al-Amri et al.[1] considered on the flow of magnetohydrodynamic nanofluid that incorporates microorganisms, incorporating the thermophoretic drift and Brownian diffusion effects. They explored the influence of nanoparticle combination on magnetohydrodynamic stagnation point fluid motion influenced by mixed convection. The investigation of nanoparticle aggregation was based on two modified models, namely the Maxwell–Bruggeman and Krieger–Dougherty models by Mahmood et al. [2]. Nadeem et al. [3] probed the stagnation flow of nanomaterials dispersed in micropolar fluids past stretching sheets, emphasizing their combined impacts on thermal and material transport properties in intricate fluid flows. Khan et al. [4] inspected the influences of Cattaneo–Christov flux model on the Jeffrey nanoliquids' stagnation region fluid motion, demarcating the influence of thermal relaxation and non-Newtonian characteristics on heat and mass transfer performance. Thermal energy flux was calculated based on the Cattaneo-Christov problem. Zhou et al. [5] probed the transient stagnation region fluid motion behavior of a Casson fluid. The importance of thermal and material transport resulting from the lubricated surface was considered by Abbasi et al. [6]. Mabood et al. [7] inspected the stability and investigated the thermal behavior of HNF flow over a stretching surface with improved thermal performance over traditional nanofluids. Abbas et al. [8] developed a theoretical problem to examine the flow dependent on temperature characteristics of power-law nanofluids along a Riga sheet by incorporating the impact of velocity slip and thermal along with non-Newtonian properties. Thermal transport phenomena in a power-law liquid subjected to non-uniform heat sink/source between two stretchable disks, spaced at a constant distance and rotating coaxially, was explored by Usman et al. [9]. Dawood et al. [10] explored thermal transport and power-law liquid flow with magnetic field and slip conditions. Makhdoum et al.[11] investigated the flow of Al_2O_3 nanoparticles across a porous stretching surface under the impact of Lorentz force. Gouran et al. [12] examined the thermal performance of a thin film on a stretched sheet affected by a porous medium and radiation. Transient axisymmetric flow in a Williamson fluid induced by a porous domain with nanoparticles interacting with a radially stretched surface was considered by Saini et al. [13]. Gulzar et al. [14] theoretically studied the enhanced thermal effects resulting from the uniform decomposition of hybrid nanoparticles suspension in water. Bilal et al. [15] considered Carreau fluid film flow over a stretching surface under magnetic field. Abbas et al. [16, 17] inspected nanofliquid in various configurations by spectral collocation. Dhairiyasamy et al. [18] analyzed the role of surface modified silver NF in improving the thermal behavior of heat pipes. Hai et al. [19] proposed a computational intelligence based hybrid approach to identify the optimal parameters for ternary hybrid nanofluids. The applications of nanofluids has been explored across various geometrical configurations [20–23]. Recent studies [24–26] have investigated the intricate performance of nanofluids under non-uniform flow and thermal conditions, with particular emphasis on the influences of magnetic fields, radiation emission, and nanoparticles concentration.

The novelty of this research lies in the numerical investigation of nanofluid flow over a lubricated boundary featuring a variable-thickness power-law lubricant layer. The model accounts for Brownian motion and thermophoresis by employing the Boungiorno model and achieves a deeper understanding of the transport of nanoparticles and its effects on mass and heat transfer. The research also takes into account viscous dissipation, heat generation, and thermal radiation and hence can be applied to thermal management systems and industrial lubrication. The governing equations are numerically solved employing the Keller Box Numerical Scheme (KBNS) to provide high accuracy in the evaluation of velocity, temperature, and concentration profiles under different lubrication effects. This study offers new theoretical and computational approaches that further our understanding of power-law lubricant interactions with nanofluids, providing real-world applications in thermal engineering, lubrication technology, and advanced coating processes.

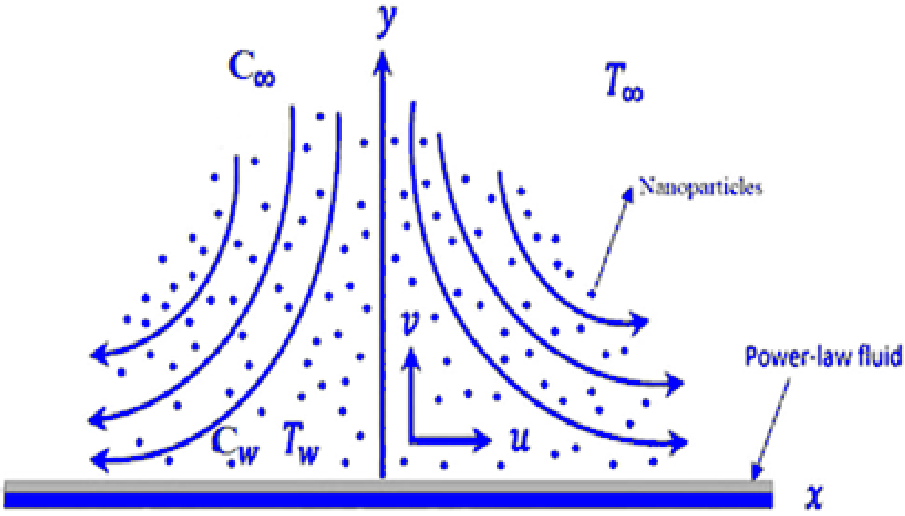

Figure 1: Geometry of the problem

3. Mathematical Formulation

Analyze a 2D, laminar, steady, and incompressible nanofluid flow within a quiescent region moving toward a stretching sheet. The sheet is layered with a thin film of lubricant, which follows the power-law rheological model; the coating has a spatially varying thickness. The wall temperature T_W and wall concentration C_W are taken as constant. Similarly, C_∞ and T_∞ represent the ambient temperature and concentration, respectively, far from the sheet. Under these conditions, the transport phenomena in the system can be modeled by the following equations. The analysis is carried out with the following assumptions [19–21]:

Continuity Equation:

$$\frac{\partial u}{\partial x} + \frac{\partial v}{\partial y} = 0, \tag{1}$$

Momentum conservation along the x-direction:

$$u\frac{\partial u}{\partial x} + v\frac{\partial u}{\partial y} = \nu\left(\frac{\partial^2 u}{\partial x^2} + \frac{\partial^2 u}{\partial y^2}\right) - \frac{1}{\rho_f}\frac{\partial p}{\partial x}, \tag{2}$$

Momentum conservation along the y-direction:

$$u\frac{\partial v}{\partial x} + v\frac{\partial v}{\partial y} = \nu\left(\frac{\partial^2 v}{\partial x^2} + \frac{\partial^2 v}{\partial y^2}\right) - \frac{1}{\rho_f}\frac{\partial p}{\partial y}, \tag{3}$$

Energy Equation:

$$u\frac{\partial T}{\partial x}+v\frac{\partial T}{\partial y} = \alpha\frac{\partial^2 T}{\partial y^2}+\tau\left[\frac{D_T}{T_\infty}\left(\frac{\partial T}{\partial y}\right)^2 + D_B\left(\frac{\partial C}{\partial y}\frac{\partial T}{\partial y} + \frac{\partial C}{\partial x}\frac{\partial T}{\partial x}\right)\right]-\frac{1}{\rho c_p}\frac{\partial q_r}{\partial y}+\frac{Q_0}{\rho c_p}(T-T_\infty)+\frac{\mu_f}{\rho c_p}\left(\frac{\partial u}{\partial y}\right)^2, \tag{4}$$

Species (Mass) Transport Equation:

$$u\frac{\partial C}{\partial x} + v\frac{\partial C}{\partial y} = D_B\left(\frac{\partial^2 C}{\partial x^2} + \frac{\partial^2 C}{\partial y^2}\right) + \frac{D_T}{T_\infty}\left[\frac{\partial^2 C}{\partial x^2} + \frac{\partial^2 C}{\partial y^2}\right], \tag{5}$$

The u and v represent the horizontal and vertical components of velocity, respectively, and ρ_f is the density of the base fluid. The fluid temperature, pressure, kinematic viscosity, nanoparticle density, and nanoparticle concentration are represented by T, p, ν, ρ_p and C respectively. D_B and D_T signify the Brownian motion and thermophoretic diffusion, respectively. In addition, Q_o is the internal heat generation term, and q_r is the thermal radiation parameter.
If $\vec{V}$ is a vector expressed in terms of its components, then it can be written as $\vec{V} = (U, V)$, where V and U represent its respective components, therefore lubricant rate is described as [8].

$$Q = \int_0^{\delta(x)} U(x, y)dy, \tag{6}$$

Implies no slip boundary condition

$$V(x, y) = 0, U(x, 0) = cx = U_w(x), \tag{7}$$

The stretching speed is indicated here by x, and the c is constant positive. We required the lubrication film to be very thin. Then

$$V(x, y) = 0, 0 \leq y \leq \delta(x), \tag{8}$$

If μ and μ_L denote nanofluids and power-law respectively, then by equating the shear stress continuity of both fluids, the interfacial condition can be expressed as

$$\mu\left(\frac{\partial u}{\partial y}\right) = \mu_L\frac{\partial U}{\partial y}, \tag{9}$$

Where μ_L is defined as

$$\mu_L = k\left(\frac{\partial U}{\partial y}\right)^{m-1}, \tag{10}$$

Here, m refers to the exponent of power law, while k denotes the flow consistency index. Equation (11) may be expressed in the following form:

$$\frac{\partial u}{\partial y} = \frac{k}{\mu}\left(\frac{1}{2Q}\right)^m \bar{U}^{2m}, \tag{11}$$

The symbol $\bar{U}$ represents the two fluids interfacial velocity. Eq. (11), in conjunction with vertical velocity continuity between the two fluids. At $y = \delta(x)$ we impose the condition

$$v = 0 = V, \tag{12}$$

The conditions specified in equations (11) and (12) can be imposed according to the thin layer of lubricant. This ensures continuity of horizontal velocity for both fluids.

$$\bar{U} = u - cx, \tag{13}$$

So Eq. (13) reduces the form

$$\frac{\partial u}{\partial y} = \frac{k}{\mu}\left(\frac{1}{2Q}\right)^m (u - cx)^{2m}, \tag{14}$$

Moreover, the following boundary specifications, which are significant to the model, are employed:

$$v = 0, C = C_w, T = T_w, aty = 0 \tag{15}$$

$$u \to u_e(x) = ax, v \to 0, C \to C_\infty, T \to T_\infty, aty \to \infty \tag{16}$$

In which ax is a ambient flow velocity. The following dimensionless quantities are expressed as follows:

$$\psi = x\sqrt{c\nu}f(\eta), \eta = \sqrt{\frac{c}{\nu}}y, \theta(\eta) = \frac{T - T_\infty}{T_w - T_\infty}, \phi(\eta) = \frac{C - C_\infty}{C_w - C_\infty}. \tag{17}$$

Applying the equation (17), the PDEs (2) to (5) along with the boundary conditions (13) to (16) are reduced to the following set of ODEs:

$$f''' + ff'' - f'^2 = -\frac{a^2}{c^2}, \tag{18}$$

$$\frac{1}{Pr}\left(1 + \frac{4}{3}Rd\right)\theta'' + N_b\theta'\phi' + f\theta' + N_t\theta'^2 + Ecf''^2 - Q\theta = 0, \tag{19}$$

$$\phi'' + Lef\phi' + \frac{N_t}{N_b}\theta'' = 0, \tag{20}$$

$$f(0) = 0, f''(0) = \beta((f'(0) - 1)^{2m}), \phi(0) = 1, \theta(0) = 1, \tag{21}$$

$$\phi(\infty) \to 0, f'(\infty) \to \frac{a}{c}, \theta(\infty) \to 0. \tag{22}$$

The Prandtl number, denoted as Pr, is defined by $Pr = \frac{\nu_f(\rho c_p)_f}{k_f}$, Eckert number represented as $Ec = \frac{u_w^2}{(cp)(T_w - T_\infty)}$, the parameter Q is used to describe the heat produced is defined by $Q = \frac{Q_0}{c(\rho c_p)_f}$, Radiation number defined as $Rd = \frac{(4\sigma^* T_\infty^3)}{(k^* k_f)}$, the Lewis number is defined as $Le = \frac{\nu}{D_B}$, while the Brownian motion parameter is given by $N_b = \frac{(\rho d)_p D_B(C_w - C_\infty)}{(\rho d)_f \nu}$, and the thermophoretic force parameter is expressed as $N_t = \frac{(\rho d)_p D_T(T_w - T_\infty)}{(\rho d)_f T_\infty \nu}$. The $\beta = \frac{k\sqrt{\nu}}{\mu}\frac{a^{2m}x^{2m-1}}{a^{\frac{3}{2}}(2Q)^m}$, where β represents the measure of the viscous length scales relative to the lubrication length scale.

$$\beta = \frac{L_{visc}}{L_{lub}} = \frac{\sqrt{\nu/\alpha}}{(\mu/k)\sqrt{2Q}} \tag{23}$$

As indicated by equation (24), increasing the L_{lub} (lubrication length) for a fluid of low viscosity reduces the parameter β. When $\beta \to 0$, the system satisfies the condition (full-slip) $f(0) = 0$; on the other hand, $\beta \to 1$, enforces the condition (no-slip) $f'(0) = 1$. This highlights β measures the slip induced by the lubricant.

$$\tau_w = \mu \left(\frac{\partial u}{\partial y}\right)_{y=0}, j_w = -D_B \left(\frac{\partial C}{\partial y}\right)_{y=0}, q_w = -K \left(\frac{\partial T}{\partial y}\right)_{y=0}, \tag{24}$$

Sherwood, skin friction, and Nusselt number are among the measurements that are provided by

$$Nu_x = \frac{xq_w}{k(T_w - T_\infty)}, C_f = \frac{\tau_w}{\rho u_w^2}, Sh = \frac{xj_w}{D_B(C_w - C_\infty)}, \tag{25}$$

In dimensionless coordinates, we have

$$Re_x^{(1/2)} C_f = f''(0), Re_x^{-(1/2)} Nu_x = -\theta'(0), Re_x^{-(1/2)} Sh = -\phi'(0). \tag{26}$$

4. Keller Box Numerical Scheme

Nonlinear ODEs [18] will be solved using the Keller box numerical scheme [27–29]. First, equations (18) through (20) will be reduced to first order ODEs based on the following principles.

$$f' = u \tag{27}$$

$$u' = v \tag{28}$$

$$\phi' = n \tag{29}$$

$$\phi'' = n' \tag{30}$$

$$\theta' = p \tag{31}$$

$$\theta'' = p' \tag{32}$$

Equations (18) to (20) becomes

$$v' + fv - v^2 + \frac{a^2}{c^2} = 0, \tag{33}$$

$$\frac{1}{Pr}\left(1 + \frac{4}{3}Rd\right)p' + fp + N_b pn + N_t p^2 + Ecv^2 - Q\theta = 0, \tag{34}$$

$$n' + Lefn + \frac{N_t}{N_b}p = 0, \tag{35}$$

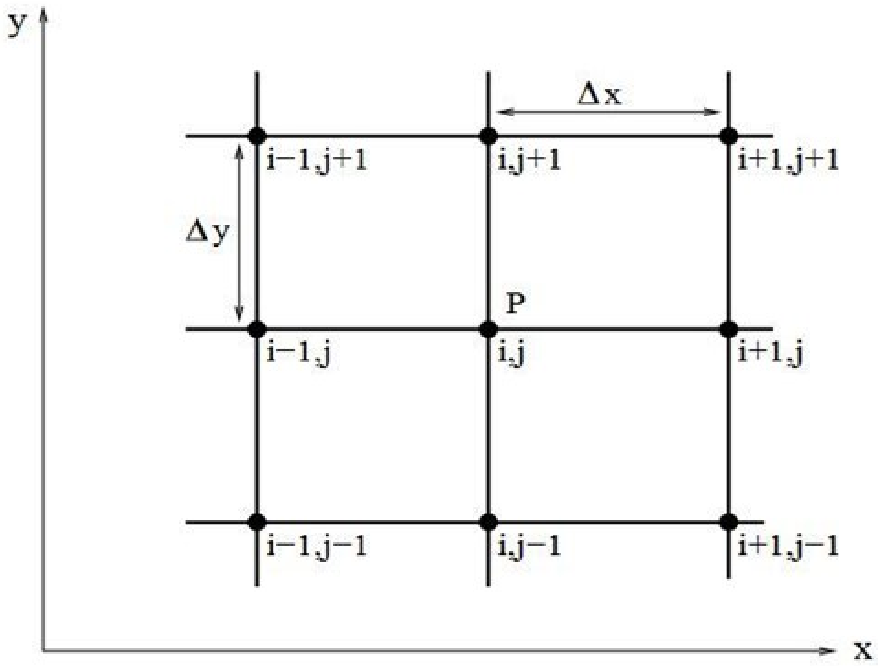

Figure 2: Domain Discretization of Nodes.

So BCs become

$$f(0) = 0, v(0) = \beta(u(0) - 1)^{2m}, \theta(0) = 1, \phi(0) = 1, \tag{36}$$

$$f'(\infty) \to \frac{a}{c}, \phi(\infty) \to 0, \theta(\infty) \to 0. \tag{37}$$

Discretization is a necessary step in solving differential equations. Figure 2 shows the procedure for discretization of domain in Keller box technique.

$$\frac{f_j - f_{j-1}}{h_j} = \frac{u_j - u_{j-1}}{2} \tag{38}$$

$$f_j - f_{j-1} - \frac{h_j}{2}(u_j - u_{j-1}) = 0, \tag{39}$$

$$\frac{u_j - u_{j-1}}{h_j} = \frac{v_j - v_{j-1}}{2} \tag{40}$$

$$u_j - u_{j-1} - \frac{h_j}{2}(v_j - v_{j-1}) = 0, \tag{41}$$

$$\frac{\phi_j - \phi_{j-1}}{h_j} = \frac{n_j - n_{j-1}}{2} \tag{42}$$

$$\phi_j - \phi_{j-1} - \frac{h_j}{2}\left(n_j - n_{j-1}\right) = 0, \tag{43}$$

$$\frac{\theta_j - \theta_{j-1}}{h_j} = \frac{p_j - p_{j-1}}{2} \tag{44}$$

$$\theta_j - \theta_{j-1} - \frac{h_j}{2}\left(p_j - p_{j-1}\right) = 0, \tag{45}$$

using equations (38) to (45) in equations (33), (34) and (35) we get

$$v_j - v_{j-1} + \frac{h_j}{4}\left(v_j + v_{j-1}\right) - \frac{h_j}{2}\left(f_j + f_{j-1}\right)\left(v_j - v_{j-1}\right)^2 + \frac{a^2}{c^2} = 0, \tag{46}$$

$$\begin{aligned} &\frac{1}{Pr}\left(1 + \frac{4}{3}Rd\right)\left(p_j - p_{j-1}\right) + \frac{N_t h_j}{4}\left(p_j + p_{j-1}\right)^2 + \frac{h_j}{4}\left(f_j + f_{j-1}\right)\left(p_j + p_{j-1}\right) \\ &+ \frac{N_b h_j}{4}\left(p_j + p_{j-1}\right)\left(n_j + n_{j-1}\right) + \frac{Ech_j}{4}\left(v_j + v_{j-1}\right)^2 - \frac{Qh_j}{2}\left(\theta_j + \theta_{j-1}\right) = 0, \end{aligned} \tag{47}$$

$$n_j - n_{j-1} + \frac{Leh_j}{4}\left(f_j + f_{j-1}\right)\left(n_j + n_{j-1}\right) + \frac{N_t}{N_b}\left(p_j + p_{j-1}\right) = 0, \tag{48}$$

Newton's method for Linearization

$$f_j^{(k+1)} = f_j^{(k)} + \delta f_j^{(k)} \tag{49}$$

$$u_j^{(k+1)} = u_j^{(k)} + \delta u_j^{(k)} \tag{50}$$

$$\phi_j^{(k+1)} = \phi_j^{(k)} + \delta \phi_j^{(k)} \tag{51}$$

$$\theta_j^{(k+1)} = \theta_j^{(k)} + \delta \theta_j^{(k)} \tag{52}$$

$$n_j^{(k+1)} = n_j^{(k)} + \delta n_j^{(k)} \tag{53}$$

$$p_j^{(k+1)} = p_j^{(k)} + \delta p_j^{(k)} \tag{54}$$

So equations (49) to (54) becomes

$$\delta f_j - \delta f_{j-1} - \frac{h_j}{2}\left(\delta u_j - \delta u_{j-1}\right) = (R_1)j \tag{55}$$

$$\delta u_j - \delta u_{j-1} - \frac{h_j}{2}\left(\delta v_j - \delta v_{j-1}\right) = (R_2)j \tag{56}$$

$$\delta \theta_j - \delta \theta_{j-1} - \frac{h_j}{2}\left(\delta p_j - \delta p_{j-1}\right) = (R_3)j \tag{57}$$

$$\delta \phi_j - \delta \phi_{j-1} - \frac{h_j}{2}\left(\delta n_j - \delta n_{j-1}\right) = (R_4)j \tag{58}$$

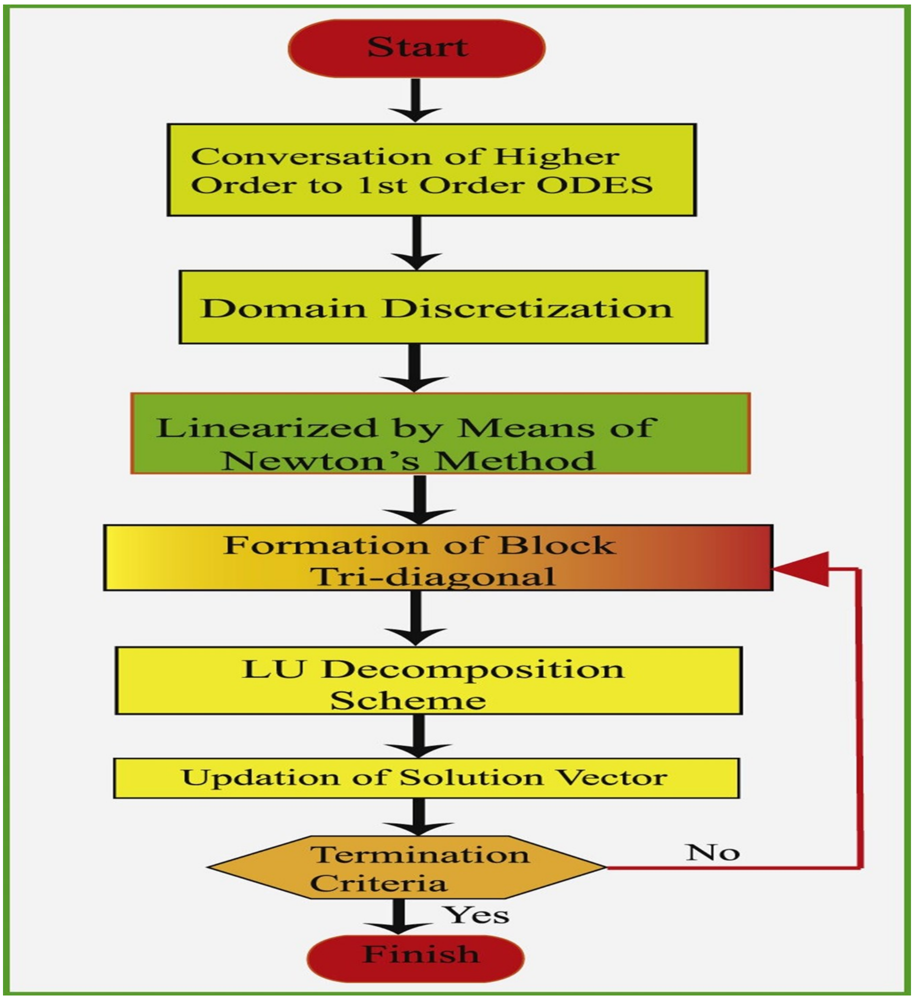

Figure 3: Flow chart of Keller Box Numerical Scheme.

So, equation (46) becomes

$$\left(1+\frac{h_j f_{j-\frac{1}{2}}}{2}-\frac{h_j v_{j-\frac{1}{2}}}{2}\right)\delta v_j+\left(-1-\frac{h_j f_{j-\frac{1}{2}}}{2}-\frac{h_j v_{j-\frac{1}{2}}}{2}\right)\delta v_{j-1}+\left(\frac{h_j v_{j-\frac{1}{2}}}{2}\right)\delta f_j$$
$$+\left(-\frac{h_j v_{j-\frac{1}{2}}}{2}\right)\delta f_{j-1}=-v_j+v_{j-1}+\frac{h_j v^2_{j-\frac{1}{2}}}{2}-\frac{a^2}{c^2}h_j, \tag{59}$$

$$[A_1]\delta v_j+[A_2]\delta v_{j-1}+[A_3]\delta f_j+[A_4]\delta f_{j-1}=(R_5)_j, \tag{60}$$

So, equation (47) becomes

$$\left(1+\frac{4}{3}Rd+\frac{h_j Prf_{j-\frac{1}{2}}}{2}+\frac{N_b p_{j-\frac{1}{2}}}{2}+\frac{N_t}{2}\right)\delta p_j+\left(-1-\frac{4}{3}Rd+\frac{h_j Prf_{j-\frac{1}{2}}}{2}-\frac{N_b n_{j-\frac{1}{2}}}{2}+\frac{N_t}{2}\right)\delta p_{j-1}$$

$$+\left(\frac{h_jPrp_{j-\frac{1}{2}}}{2}\right)\delta f_j+\left(\frac{h_jPrf_{j-\frac{1}{2}}}{2}\right)\delta f_{j-1}+\left(\frac{N_bp_{j-\frac{1}{2}}}{2}\right)\delta n_j+\left(\frac{N_bp_{j-\frac{1}{2}}}{2}\right)\delta n_{j-1}+\left(\frac{Qh_j}{2}\right)\delta\theta_j$$
$$+\left(\frac{Qh_j}{2}\right)\delta\theta_{j-1}+\left(\frac{Ech_j}{2}\right)\delta v_j+\left(\frac{Ech_j}{2}\right)\delta v_{j-1}=-\left(1+\frac{4}{3}Rd\right)(p_j-p_{j-1})+Ec\left(\frac{v_{j-\frac{1}{2}}}{2}\right)$$
$$-h_jPr\left[f_{j-\frac{1}{2}}p_{j-\frac{1}{2}}+N_b\left(f_{j-\frac{1}{2}}f_{j-\frac{1}{2}}\right)+N_t\left(\frac{p_{j-\frac{1}{2}}}{2}\right)+Q\frac{\theta_j-\theta_{j-1}}{2}\right], \tag{61}$$

$$[B_1]\delta p_j+[B_2]\delta p_{j-1}+[B_3]\delta f_j+[B_4]\delta f_{j-1}+[B_5]\delta n_j+[B_6]\delta n_{j-1}+[B_7]\delta\theta_j+[B_8]\delta\theta_{j-1}$$
$$+[B_8]\delta v_j+[B_9]\delta v_{j-1}=(R_6)_j, \tag{62}$$

So, equation (48) becomes

$$\delta n_j\left[1+h_j(f_{j-1})\right]-\delta n_{j-1}\left[1+h_j(f_{j-1})\right]+\delta p_j\left[\frac{N_t}{N_b}\right]-\delta p_{j-1}\left[\frac{N_t}{N_b}\right]+\delta f_j\left[h_j\left(\frac{Le}{2}\right)\right]$$
$$-\delta f_{j-1}\left[h_j\frac{Le}{2}\right]=(n_j-n_{j-1})+\left[\frac{N_t}{N_b}\right](p_j-p_{j-1})+Le\left(f_j-f_{j-1}\right), \tag{63}$$

$$[C_1]\delta n_j+[C_2]\delta n_{j-1}+[C_3]\delta p_j+[C_4]\delta p_{j-1}+[C_5]\delta f_j+[C_6]\delta f_{j-1}=(R_7)_j, \tag{64}$$

Where

$$[A_1]=\left(1+\frac{h_jf_{j-\frac{1}{2}}}{2}-\frac{h_jv_{j-\frac{1}{2}}}{2}\right)=-[A_2];-[A_4]=[A_3]=\left(\frac{h_jv_{j-\frac{1}{2}}}{2}\right);$$
$$[B_1]=\left(1+\frac{4}{3}Rd+\frac{h_jPrf_{j-\frac{1}{2}}}{2}+\frac{N_bp_{j-\frac{1}{2}}}{2}+\frac{N_t}{2}\right)=-[B_2];[B_3]=\left(\frac{h_jPrp_{j-\frac{1}{2}}}{2}\right);$$
$$-[B_6]=[B_5]=[B_3]=\left(\frac{N_bp_{j-\frac{1}{2}}}{2}\right);-[B_8]=[B_7]=\left(\frac{Qh_j}{2}\right);[B_9]-[B_4]=\delta v_j=-[B_{10}];$$
$$[C_1]=[1+h_j(f_{j-1})]=-[C_2];[C_3]=[N_t/N_b]=-[C_4];[C_5]=h_j\frac{Le}{2}]=-[C_6];$$
$$(R_1)j=h_ju_{j-\frac{1}{2}}+f_{j-1}-f_j;(R_2)j=h_jv_{j-\frac{1}{2}}+u_{j-1}-u_j;(R_3)j=\theta_{j-1}-\theta_j+h_jp_{j-\frac{1}{2}};$$
$$(R_4)j=\phi_{j-1}-\phi_j+h_jn_{j-\frac{1}{2}};(R_5)_j=-v_j+v_{j-1}+\frac{h_jv^2_{j-\frac{1}{2}}}{2}-\frac{a^2}{c^2}h_j;$$
$$(R_6)_j=-\left(1+\frac{4}{3}Rd\right)(p_j-p_{j-1})-h_jPr\left[f_{j-\frac{1}{2}}p_{j-\frac{1}{2}}+N_b(p_{j-\frac{1}{2}}f_{j-\frac{1}{2}})+N_t\frac{p_{j-\frac{1}{2}}}{2}+Q\left(\frac{\theta_j+\theta_{j-\frac{1}{2}}}{2}\right)\right];$$
$$+Ec\left(\frac{v_{j-\frac{1}{2}}}{2}\right);(R_7)_j=(n_j-n_{j-1})+\left[\frac{N_t}{N_b}\right](p_j-p_{j-1})+Le\left(f_j-f_{j-1}\right). \tag{65}$$

So the BC's becomes

$$\delta f_0=0,\delta v_0=\beta(\delta u_0-1)^{2m},\delta\theta_0=1,\delta\phi_0=1,$$
$$\delta u_j\to 0,\delta\theta_j\to 0,\delta\phi_j\to 0. \tag{66}$$

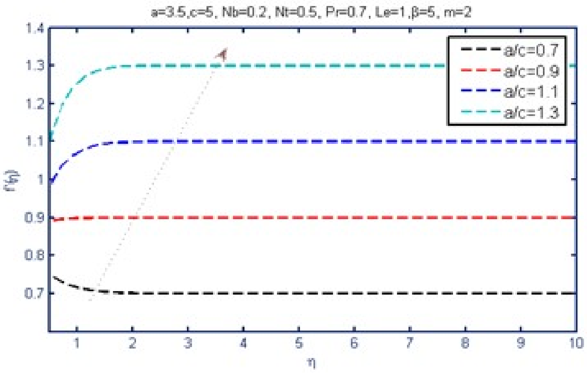

Figure 4: Impact for various values of a/c on velocity.

4.1. The Block-elimination method

Equation (51-58) give block-tridiagonal structure for $\varrho_j = -\frac{h_j}{2}$
Matrix-vectors can be expressed as

$$A\delta = r, \tag{67}$$

Wherein

$$A = \begin{bmatrix} [A_1] & [C_1] & & & \\ [B_2] & [A_2] & [C_2] & & \\ & \ddots & \ddots & \ddots & \\ & & [B_{J-1}] & [A_{J-1}] & [C_{J-1}] \\ & & & [B_J] & [A_J] \end{bmatrix}, \tag{68}$$

$$\delta = \begin{bmatrix} [\delta_1] \\ [\delta_2] \\ \vdots \\ [\delta_{J-1}] \\ [\delta_J] \end{bmatrix}, \quad r = \begin{bmatrix} [r_1] \\ [r_2] \\ \vdots \\ [r_{J-1}] \\ [r_J] \end{bmatrix}. \tag{69}$$

5. Results and Discussions

In fig. 4 illustrates the velocity profile for different values of a/c keeping the slip parameter $\beta = 5$. It is observed that when value of a/c increased the velocity field also increases. are discussed for the velocity profile in the figures 5 & 6. It has been observe that the $f(\eta)$ increase when the slip number β increase when the stretching ratio parameter is $a/c < 1$. The Main Reason is that free stream velocity is bigger than the Stretching velocity. Figure 5 represent that the velocity graph decline when we rise the value of β and fixed the stretching ratio parameter $a/c > 1$. At that time the stretching velocity is

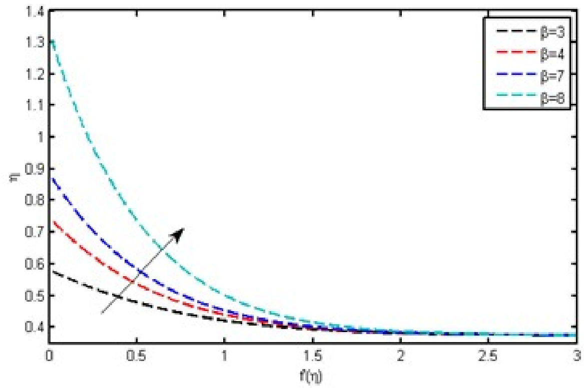

Figure 5: Impact for various values of β when $a/c = 0.3$ on velocity.

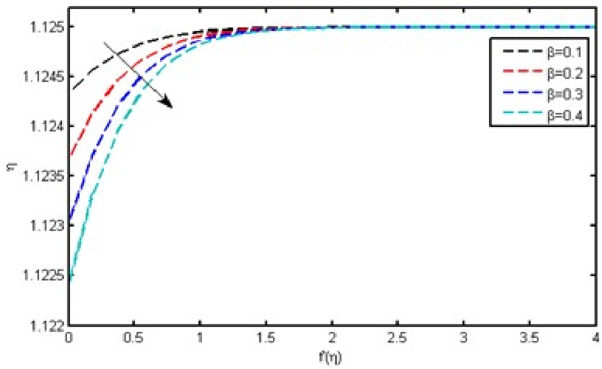

Figure 6: Impact for various values of β when $a/c = 1.12$ on velocity.

greater than the free stream velocity.
The impact of different numbers on the temperature distribution are shown in figures 7-9. In fig. 7 the thermal field declines for rising the values of viscous dissipation number Ec keeping $a/c = 0.7$ and slip parameter is $\beta = 5$. Figure 8 shows the effect of radiation parameter on thermal distribution. Increasing Rd results in increasing the temperature profile at $a/c = 0.7$ and slip parameter is $\beta = 5$. Increasing Rd will raise the friction and reducing the heat transfer so temperature graph increase. Figure 9 shows the decreasing trend in fluid temperature against increasing the generation parameter Q .
Figures 10 illustrate the impact of a/c on concentration profile ϕ. A detailed examination reveals that the concentration decreases as a/c increase in magnitude. The relationship of concentration of profile ϕ with N_b, N_t and Le is represented in Figures 11,12,13. These figures demonstrate that concentration profile of ϕ decrease with the increase in N_b and Le. And concentration profile rises with the increases of N_t. Figure 14 illustrates the impact of varying the Pr and Le on the θ. It is observed that an rise in Pr leads to decrease in the temperature of the fluid.

The table 1 displays a comparison of the $f''(0)$ values obtained by three various stud-

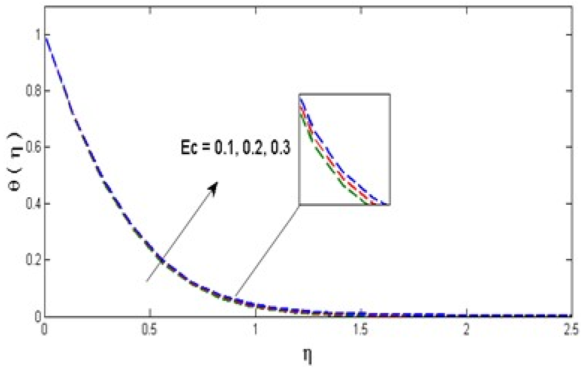

Figure 7: Impact for various values of Ec

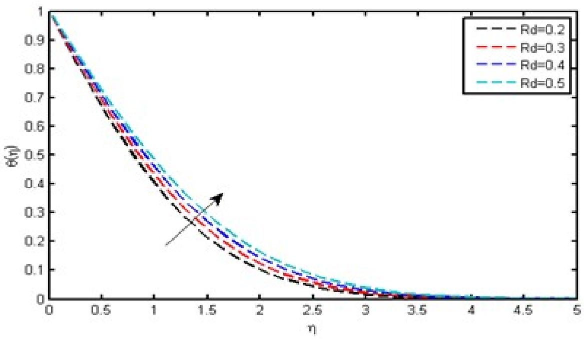

Figure 8: Impact for various values of Rd on θ.

ies: Sadiq et al. [19], Mustafa et al. [20], and the Current Study. Moreover, the table has the absolute errors between the Current Study and the other two references.

For $a/c = 0.01$, the $f''(0)$ values in all studies are close to one another with very little error of 9.99×10^{-7} when calculated against Sadiq et al. [19], and with a bit higher error of 0.000298 when calculated against Mustafa et al. [20]. In the same vein, for $a/c = 0.10$, the error against Sadiq et al. [19] is small at 9.99×10^{-6}, whereas with Mustafa et al. [20], the error is 0.000107. As a/c rises, the trend is the same, with the values of error still being relatively small. For example, when $a/c = 0.50$, the largest absolute error is 7.70×10^{-5} (in comparison to Mustafa et al. [20]), whereas at $a/c = 2.00$, the largest absolute error is 0.000159. The greatest observed discrepancy in the dataset is at $a/c = 3.00$, where the discrepancy between the Current Study and Mustafa et al. [20] is 0.000379, and the discrepancy with respect to Sadiq et al. [19] is still very small at 1.10×10^{-5}.
The table 2 presents a comparative study of $-\theta'(0)$ values for various values of Pr and a/c, keeping in view the findings of Sadiq et al. [19], Mustafa et al. [20], and the Current Study. The table also presents the absolute errors between the Current Study and the reference studies.
For $Pr = 1.0$ and $a/c = 0.1$, the Current Study indicates an extremely small error of

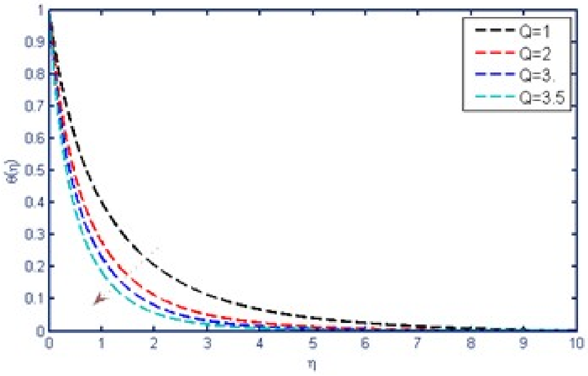

Figure 9: Impact for various values of Q on θ.

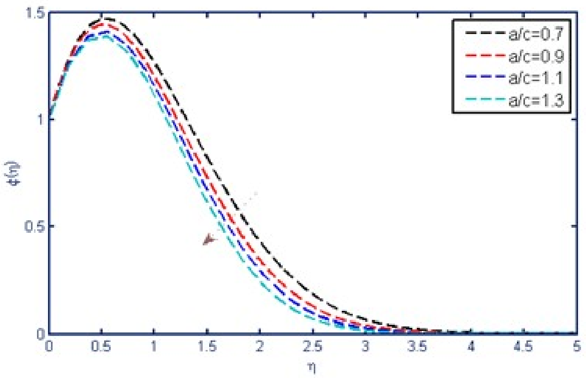

Figure 10: Impact for various values of a/c on ϕ.

1.10×10^{-6} compared to Sadiq et al. [19], and the difference with Mustafa et al. [20] is a bit greater at 0.0010311. The same trend is seen for $a/c = 0.2$, where the error with Sadiq et al. [19] is still very low at 1.10×10^{-6}, and with Mustafa et al. [20] is 0.0003021. For $a/c = 0.5$, the error figures are even lower, with a highest deviation of just 3.80×10^{-6} from Mustafa et al. [20]. For $Pr = 1.5$, the variations still remain negligible. For $a/c = 0.1$, the error in comparison to Sadiq et al. [19] is 4.99×10^{-7}, and the error in comparison to Mustafa et al. [20] is 2.35×10^{-5}. Likewise, for $a/c = 0.2$, the variation is negligible, with errors of 1.00×10^{-7} and 7.10×10^{-6} in comparison to Sadiq et al. [19] and Mustafa et al. [20], respectively.

In general, the Current Study presents a high level of congruence with the reference studies with slight discrepancies which can be attributed to numerical accuracy, computation strategies, or the difference in rounding. The values of error are very low, and thus, the Current Study presents precise and reliable findings according to prior work.

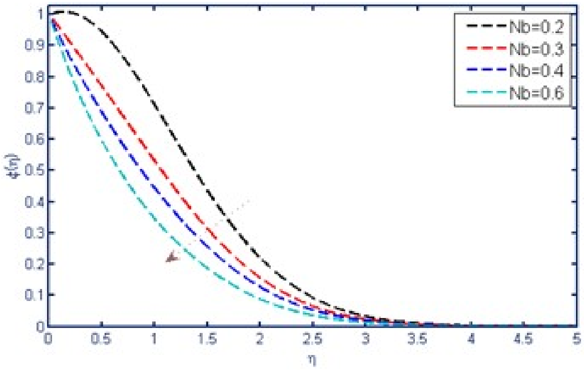

Figure 11: Impact for various values of Nb on ϕ.

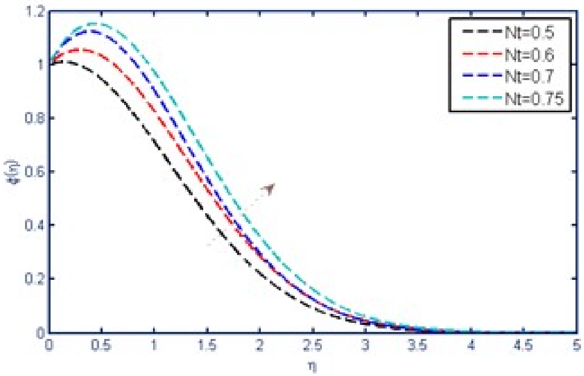

Figure 12: Impact for various values of Nt on ϕ.

6. Conclusion

In the present investigation, we analyzed the flow of nanoliquid in a stagnation-point theory through an unsteady stretching sheet. Thin layer of a power law liquid that coats the surface The normalized governing equations (the dimensionless form of governing equations) were obtained by using a suitable transformation. Keller Box numerical simulation also yields a comparable solution. The influence of the involved parameters on the quantities of interest is examined in detail. Key results from the inquiries include:
The velocity of the nanofluid is raised with an increasing a/c and β. It is observed that the temperature of the liquid decreases for grater values of a/c, β, Pr and Le and it will increase by increasing both N_b and N_t. An increased in the a/c, β, Pr, Le and N_b caused to reduce concentration of fluid while it is decreased for high value of N_t. By raising a/c, $f''(0)$ improves, and by raising β, it decreases. $-\theta'(0)$ grows as a/c, β and Pr increases, but decreases with higher values of N_t, N_b and Le. $-\phi'(0)$ increases with higher of a/c, β, N_b and Le, and while it decreases with increasing N_t and Pr.
In spite of these useful results, some shortfalls need to be recognized. The analysis invokes a steady-state, laminar, and incompressible flow with a power-law lubricant, which possibly

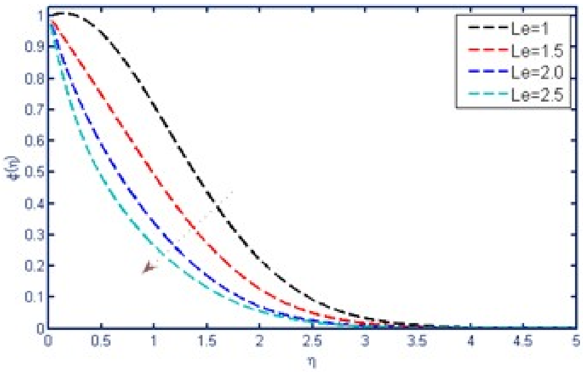

Figure 13: Impact for various values of Le on ϕ.

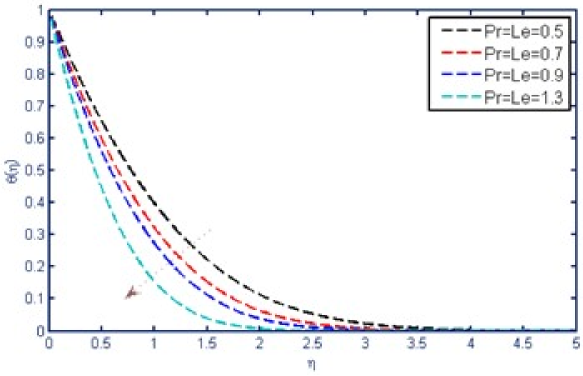

Figure 14: Impact for various values Pr and Le on profile θ.

does not depict transient or turbulence effects that arise in actual problems. The theory also ignores the aggregation of the nanoparticles, the roughness of the surface, and thermal non-equilibrium influences, which tend to affect real heat and mass transfer behavior. Furthermore, the effect of external forces like electromagnetic fields or buoyancy-induced convection is not taken into account. Such limitations can reduce the applicability of the results, especially in intricate industrial or natural fluid flow settings.

Further studies could expand this research by adding time-dependent flow conditions, turbulence models, and nanofluid multi-phase interactions, which would increase the relevance of the results to a wider variety of engineering and industrial problems. However, the current work establishes a firm theoretical and numerical foundation for exploring the impact of lubrication on nanofluid flow, providing new insight into thermal management and lubrication technologies.

Conflict of Interest

No conflict of interest are associated with the publication of this research work.

Table 1: Comparison of the numerical values of $f''(0)$.

a/c	**Sadiq et al. [30]**	**Mustafa et al. [31]**	**Current Study**	Error (Current – Sadiq)	Error (Current – Mustafa)
0.01	-0.998527	-0.99823	-0.998528	9.999999999177334e-07	0.00029800000000002047
0.10	-0.969423	-0.96954	-0.969433	9.99999999995449e-06	0.00010699999999996823
0.50	-0.667264	-0.66735	-0.667273	9.000000000036756e-06	7.699999999999374e-05
2.00	2.01750	2.01767	2.017511	1.09999999997612e-05	0.00015900000000002024
3.00	4.72925	4.72964	4.729261	1.09999999997612e-05	0.00037899999999968514

Table 2: Comparison of the numerical values of $-\theta'(0)$ for $N_b = N_t = 0$.

Pr	a/c	**Sadiq et al. [30]**	**Mustafa et al. [31]**	**Current Study**	Error (Current – Sadiq)	Error (Current – Mustafa)
1.0	0.1	0.603186	0.602156	0.6031871	1.09999999997612e-06	0.0010310999999999515
	0.2	0.624768	0.624467	0.6247691	1.09999999997612e-06	0.00030209999999997184
	0.5	0.692456	0.692460	0.6924562	2.0000000000575113e-07	3.7999999999982492e-06
1.5	0.1	0.776825	0.776802	0.7768255	4.999999999588667e-07	2.3499999999954113e-05
	0.2	0.797129	0.797122	0.7971291	1.0000000005838672e-07	7.100000000037632e-06

Data Availability:

No datasets were used or analyzed for the current study.

References

[1] Fahad Al-Amri and M Muthtamilselvan. Stagnation point flow of nanofluid containing micro-organisms. *Case Studies in Thermal Engineering*, 21:100656, 2020.

[2] Zafar Mahmood, Sharifah E Alhazmi, Awatif Alhowaity, Riadh Marzouki, Nadir Al-Ansari, and Umar Khan. Mhd mixed convective stagnation point flow of nanofluid past a permeable stretching sheet with nanoparticles aggregation and thermal stratification. *Scientific Reports*, 12(1):16020, 2022.

[3] S Nadeem, Asma Amin, and Nadeem Abbas. On the stagnation point flow of nanomaterial with base viscoelastic micropolar fluid over a stretching surface. *Alexandria Engineering Journal*, 59(3):1751–1760, 2020.

[4] Sohail A Khan, T Hayat, and A Alsaedi. Cattaneo christov (cc) heat and mass fluxes in stagnation point flow of jeffrey nanoliquids by a stretched surface. *Chinese Journal of Physics*, 76:205–216, 2022.

[5] Jian-Cun Zhou, Awatef Abidi, Qiu-Hong Shi, M Riaz Khan, Aysha Rehman, Alibek Issakhov, and Ahmed M Galal. Unsteady radiative slip flow of mhd casson fluid over a permeable stretched surface subject to a non-uniform heat source. *Case Studies in Thermal Engineering*, 26:101141, 2021.

[6] A Abbasi, W Farooq, Sami Ullah Khan, and Iqra Riaz. Lubricated surface oblique stagnation point flow of second-grade fluid with heat and mass transfer phenomenon:

applications to hydraulic systems. *Waves in Random and Complex Media*, pages 1–20, 2023.

[7] F Mabood and AT Akinshilo. Stability analysis and heat transfer of hybrid cu-al2o3/h2o nanofluids transport over a stretching surface. *International Communications in Heat and Mass Transfer*, 123:105215, 2021.

[8] Nadeem Abbas, Khalil Ur Rehman, Wasfi Shatanawi, and Kamaleldin Abodayeh. Mathematical model of temperature-dependent flow of power-law nanofluid over a variable stretching riga sheet. *Waves in random and complex media*, pages 1–18, 2022.

[9] Usman, Ping Lin, and Abuzar Ghaffari. Steady flow and heat transfer of the power-law fluid between two stretchable rotating disks with non-uniform heat source/sink: Usman et al. *Journal of Thermal Analysis and Calorimetry*, 146(4):1735–1749, 2021.

[10] Muhammad Dawood, Muhammad Yousaf, Shafiq Ahmad, and Salman Zeb. Non-newtonian power-law fluids with variable magnetic field and slip conditions. *Proceedings of the Institution of Mechanical Engineers, Part E: Journal of Process Mechanical Engineering*, 237(3):793–804, 2023.

[11] Basim M Makhdoum, Zafar Mahmood, Bandar M Fadhl, Musaad S Aldhabani, Umar Khan, and Sayed M Eldin. Significance of entropy generation and nanoparticle aggregation on stagnation point flow of nanofluid over stretching sheet with inclined lorentz force. *Arabian Journal of Chemistry*, 16(6):104787, 2023.

[12] S Gouran, J Vahidi, H Akbari, and SE Ghasemi. Thermal radiation and porous medium effects on a thin liquid film over a stretching sheet: A numerical comparative study. *Case Studies in Thermal Engineering*, 52:103753, 2023.

[13] Sonu Kumar Saini, Rashmi Agrawal, and Pradeep Kaswan. Activation energy and convective heat transfer effects on the radiative williamson nanofluid flow over a radially stretching surface containing joule heating and viscous dissipation. *Numerical Heat Transfer, Part A: Applications*, 85(15):2534–2557, 2024.

[14] S Gulzar, Kamel Al-Khaled, W Farooq, A Abbasi, and Sami Ullah Khan. A thin layer lubricant surface applications due to nonlinear radiated hybrid nanoparticles with orthogonal stagnation point flow. *International Journal of Modelling and Simulation*, 45(3):853–865, 2025.

[15] Muhammad Bilal, Anwar Saeed, Taza Gul, Muhammad Rehman, and Amir Khan. Thin-film flow of carreau fluid over a stretching surface including the couple stress and uniform magnetic field. *Partial Differential Equations in Applied Mathematics*, 4:100162, 2021.

[16] Tasawar Abbas. Magnetohydrodynamic flow of a hybrid nanofluid over an exponentially stretching sheet with joule heating and slip conditions using spectral collocation method with legendre wavelets. *Multiscale and Multidisciplinary Modeling, Experiments and Design*, 8(1):125, 2025.

[17] Tasawar Abbas. Numerical simulation of heat transfer in williamson hybrid nanofluid (m g o-a g/water) flow with viscous dissipation effects. *Multiscale and Multidisciplinary Modeling, Experiments and Design*, 8(6):293, 2025.

[18] Ratchagaraja Dhairiyasamy, Deepika Gabiriel, Wasurat Bunpheng, and Chan Choon

Kit. Impact of silver nanofluid modifications on heat pipe thermal performance. *Journal of Thermal Analysis and Calorimetry*, 150(3):2079–2098, 2025.

[19] Tao Hai, Ali Basem, As' ad Alizadeh, Pradeep Kumar Singh, Husam Rajab, Chemseddine Maatki, Nidhal Becheikh, Lioua Kolsi, Narinderjit Singh Sawaran Singh, and H Maleki. Optimizing ternary hybrid nanofluids using neural networks, gene expression programming, and multi-objective particle swarm optimization: a computational intelligence strategy. *Scientific Reports*, 15(1):1986, 2025.

[20] Salma Khalil, Tasawar Abbas, and R Nawaz. Study of hybrid nanofluid flow in a porous medium over an exponentially stretching sheet under joule heating and thermal radiation: Finite difference. *Nano-Structures & Nano-Objects*, 40:101350, 2024.

[21] Faisal Mumtaz, Tasawar Abbas, Adil Jhangeer, and Ijaz Ali. Analysis of thermal significances of nanofluids in inclined magnetized flow with joule heating source and slip effects. *Nano-Structures & Nano-Objects*, 40:101349, 2024.

[22] Aaqib Majeed, Sami Ullah Khan, Tasawar Abbas, M Ijaz Khan, Barno Sayfutdinovna Abdullaeva, Emad A Ismail, and Fuad A Awwad. Bidirectional bioconvective flow of casson–micropolar nanofluid due to porous riga surface with heat generation effects. *AIP Advances*, 14(11), 2024.

[23] Muhammad Shoaib Kamran, Muhammad Irfan, Muavia Mansoor, Taseer Muhammad, and Qazi Mahmood Ul-Hassan. Significance of cattaneo–christov heat flux theory and convective heat transport on maxwell nanofluid flow. *ZAMM-Journal of Applied Mathematics and Mechanics/Zeitschrift für Angewandte Mathematik und Mechanik*, 104(10):e202400006, 2024.

[24] Mutasem Z Bani-Fwaz, Adnan, Sumaira Fayyaz, Nidhish Kumar Mishra, Zafar Mahmood, Sami Ullah Khan, and Muhammad Bilal. Investigation of unsteady nanofluid over half infinite domain under the action of parametric effects and epnm. *Journal of Thermal Analysis and Calorimetry*, 150(4):2975–2988, 2025.

[25] Ammara Islam, Zafar Mahmood, and Umar Khan. Double-diffusive stagnation point flow over a vertical surface with thermal radiation: assisting and opposing flows. *Science Progress*, 106(1):00368504221149798, 2023.

[26] Safyan Mukhtar, Siddra Rana, Muavia Mansoor, Tayyaba Arooj, Qazi Mahmood Ul Hassan, and Rasool Shah. Mhd viscoelastic nanofluid flow across an extended plate using mixed convection and thermal radiation. *Frontiers in Energy Research*, 12:1275652, 2024.

[27] Yu-Ming Chu, M Ijaz Khan, Tasawar Abbas, Maawiya Ould Sidi, Khalid Abdulkhaliq M Alharbi, Umar F Alqsair, Sami Ullah Khan, M Riaz Khan, and MY Malik. Radiative thermal analysis for four types of hybrid nanoparticles subject to non-uniform heat source: Keller box numerical approach. *Case Studies in Thermal Engineering*, 40:102474, 2022.

[28] Omar T Bafakeeh, Bilal Ahmad, Skeena Noor, Tasawar Abbas, Sami Ullah Khan, Muhammad Ijaz Khan, Samia Elattar, Sayed M Eldin, Mowffaq Oreijah, and Kamel Guedri. Nonlinear thermal diffusion and radiative stagnation point flow of nanofluid with viscous dissipation and slip constrains: Keller box framework applications to

micromachines. *Micromachines*, 13(11):1839, 2022.

[29] Tasawar Abbas, Kamel Al-Khaled, Ahmed Haseeb Raza, Mohamed Ayadi, Wathek Chammam, and Sami Ullah Khan. Inclined magnetized flow of radioactive nanoparticles with exponential heat source and slip effects: Keller box simulations. *Journal of Nanofluids*, 12(2):571–579, 2023.

[30] Muhammad Noveel Sadiq, Muhammad Sajid, Tasawar Abbas, Khalid Mahmood, Sammar Bashir, and Waqar Mahmood. Numerical simulation for flow and heat transfer of a nanofluid over lubricated stretchable surface. *Journal of Nanofluids*, 12(2):506–513, 2023.

[31] M Mustafa, T Hayat, I Pop, S Asghar, and S Obaidat. Stagnation-point flow of a nanofluid towards a stretching sheet. *International Journal of Heat and Mass Transfer*, 54(25-26):5588–5594, 2011.